# PECULIARITIES OF THE STRUCTURE OF THE GLOBAL OF THE SOLAR MAGNETIC FIELD IN 21-25 CYCLES

**© 2025 I. A. Bilenko**

*P.K. Sternberg State Astronomical Institute,*

*Lomonosov Moscow State University, Moscow, Russia.*

*e-mail: bilenko@sai.msu.ru*

Received February 23, 2025

Revised April 21, 2025

Accepted June 17, 2025

**Abstract.** Changes in the structure of the global magnetic field (GMF) in 21-24 and early 25 cycles are considered. It is shown that the GMF structures are different both in different cycles and at different phases of each cycle. Stable longitude structures formed during the periods of maximum activity are characterized by rotation with the period of Carrington revolutions (CR), which may indicate their connection with local magnetic fields. In each individual structure, two extended longitude intervals are distinguished with the dominance of fields of positive or negative polarity occupying opposite longitude intervals, which alternate in even and odd cycles. The increase in the contribution of sectoral structures with a simultaneous increase in the degree of their randomness leads to a decrease in the value of the average magnetic field strength for the CM in weak, 23-25, cycles. It is assumed that the total contribution of variations in the magnetic fields of the polar dipole, the sum of sectoral (n= m) harmonics, and tesseral ($n \neq m \neq 0$) harmonics with even values of n and odd values of m are decisive in the formation and cyclic changes of the observed sectoral structure of the GMF.

**DOI:** 10.31857/S00167940250716e4

## 1. INTRODUCTION

Systematic measurements of solar magnetic fields began in the sixties of the last century. The first studies of synoptic maps created on the basis of these observations showed that the solar magnetic fields are not uniformly distributed along the longitude, but form a complex structure [Ambrož et al., 1971; Bumba and Howard, 1969]. The structure of the magnetic field distribution changes both during each cycle and from cycle to cycle [Bumba and Howard 1969; Bumba, 1976; Hoeksema, 1991]. Subsequent studies have shown that the structural organization of magnetic fields is preserved at significant distances from the Sun and is observed in the interplanetary magnetic field in Earth's orbit. The global magnetic field (GMF) of the Sun forms the structure and determines the parameters of the interplanetary magnetic field [Hoeksema, 1991; Zherebtsov et al.,

1997]. It was shown in [Ivanov and Obridko, 2014] that large-scale magnetic fields play an important role in the organization of all solar activity. They influence flares and eruptive processes [Bumba and Obridko, 1969; Fainstein and Ivanov, 2010]. Changes in the structure of solar magnetic fields are reflected in various phenomena of solar activity, such as coronal mass ejections [Bilenko, 2014]. In the solar corona, the structure of the SMF and all its changes are traced by the dynamics of coronal holes [Obridko and Shelting, 1989; Insley et al., 1995; Sanchez-Ibarra and Barraza-Paredes, 1992; McIntosh, 2003; Bilenko and Tavastsherna, 2016, 2017].

The structure of the GMF is best manifested in the magnetic fields calculated at the source surface. The structure of the GMF changes from zonal in the minima of solar activity to sectoral in the maxima of each cycle. However, it is important to note that the source of the formation and cyclic evolution of the GMF structure is currently unknown. The hypothesis that a possible cause of the appearance of the observed structures and their dynamics may be Rossby waves generated at the base of the convective zone of the Sun [Tikhomolov, 1995] seems interesting. In the paper by Bilenko [2020], it was shown that the time of existence of HMP structures of different scales, the moments of their formation and reorganization coincide with the similar dynamics of Rossby waves of different frequencies.

The purpose of this study is to further consider the structural organization of solar magnetic fields and its variations in 21-24 and the first half of the 25th solar activity cycle.

## 2. DATA USED

We consider magnetic field data for the period of complete cycles 21-24 and the beginning of cycle 25 (May 1976 through December 2024, corresponding to 1642-2292 Carrington revolutions (CRs)). The synoptic maps of large-scale photospheric magnetic fields (LMPF) and fields calculated at the source surface (r= 2.5Rs) of the Wilcox Solar Observatory (WSO) [Hoeksema and Scherrer, 1986] were used for the analysis. Each synoptic map contains information about the full CM (27.2753 days), and is a longitude-latitude distribution of magnetic field strength values represented by a 72×30 array.

The values of the harmonic coefficients of the spherical harmonic decomposition of the GMF were also obtained from the WSO data site [Zhao, Xuepu and Hoeksema, 1993].

## 3. CYCLIC VARIATIONS OF THE STRUCTURE OF THE GLOBAL MAGNETIC FIELD OF THE SUN

The CPMF structurization is very weakly manifested at the photospheric level (Fig. 1a). When smoothed over several CMs, it becomes more pronounced (Fig. 1b), and it is most clearly visible on synoptic maps and, accordingly, the longitude-time diagram of the magnetic field distribution calculated at the source surface (Fig. 1c). It follows from Fig. 1c that the size, duration of quasi-stable existence, the character of rotation, and the variation of the intensity in each

individual unipolar structure are different in different cycles. The structures also differ in the minimum, growth, maximum, and decline phases of each individual cycle. Long-long structures with increased values of the magnetic field strength begin to form at the phases of solar activity growth and continue to exist during the maximum and beginning of the decline of each cycle during the period of dominance of the sectoral structure of the Sun's GMF. These structures are characterized by rotation with the CM period, which may indicate their connection with local magnetic fields. In each individual structure, two extended longitude intervals are distinguished, one of which is dominated by magnetic fields of positive polarity and the other by negative polarity. Each pair of such longitude intervals dominated by magnetic fields of positive and negative polarity occupies, approximately, in the same CMs, opposite longitude intervals, which alternate in even and odd cycles. Table 1 summarizes the following parameters for each structure: the designation number shown in Fig. 1c, the time of existence (t) in the CMs, the range of longitudes dominated by positive (L+) and negative (L-) magnetic and fields in degrees, and the maximum strengths of positive (Bmax+) and negative (Bmax-) magnetic fields calculated at the source surface (2.5 Rs). Since 0 and 360 degrees of longitude are neighboring longitudes on the Sun's sphere, two longitude intervals are given in the table for structures of the same polarity overlapping these longitudes. All values of longitudes are approximate, as structures are not exact geometrical figures. On unipolar structures there are inclusions of magnetic fields of opposite polarity. Parts of neighboring structures can find each other. In each cycle, structures with increased values of the magnetic field and with no or minimal drift in longitude were chosen. In different cycles, the longitude intervals occupied by magnetic fields of opposite polarity are different both in longitude and in the time of their existence and they are not always equal to 180 degrees, as the longitude diagrams were obtained by averaging synoptic maps of magnetic fields by latitude. During the period of the maximum in each cycle, one can observe sharp, within 1-3 CM, changes in the structure of the magnetic field distribution [Bilenko, 2014; Bilenko and Tavastsherna, 2016]. At longitude intervals dominated by magnetic fields of, for example, positive polarity, there is a change from dominance of magnetic fields to fields of negative polarity, and at the corresponding longitude intervals dominated by magnetic fields of negative polarity, there is an equally rapid change from dominance of magnetic fields to fields of positive polarity. However, these structural changes do not affect the alternation of the dominance of the magnetic field polarity dominance of the structures in even and odd cycles. In high, 21 and 22 cycles, the structures are clearer than in low, 23-25 cycles.

Fig. 2a-c shows the variations of the average magnetic field strength calculated for each CM using the corresponding diagrams of Fig. 1 for the fields of positive and negative polarity and the sum of their moduli (thin solid lines) and averaged over 13 CMs (thick solid lines for the magnetic fields of positive and negative polarity and dashed line for the sum of their moduli). Fig. 2a-c shows

that the maximum values of the magnetic field strength are higher in the high, 21, and 22 cycles. The duration of the structures does not reveal an unambiguous correspondence with the cycle height. The peaks of positive and negative polarity magnetic field strengths in Fig. 2a-c coincide with specific structures in Fig. 1c. The magnetic field in each structure does not change smoothly, but in the form of separate pulses, forming summarily two maximum increases in each cycle. At the same time, the second peak in the GMF values (Fig. 2c), occurring in the decline phase, is higher than the first one in each cycle. According to this pattern, cycle 25 should be higher than cycle 24. A decrease in the maximum values of the magnetic field strength in the structures from cycle 21 to 25 is observed (see Table 1).

The variations of the variability coefficient of the structure of the longitude distribution of magnetic fields on the source surface [KLON, Bilenko, 2014], are shown in Fig. 2d. The method of calculating the KLON coefficient is as follows. When the structure of the HMP is stable, the distribution of magnetic fields of positive and negative polarity does not change much during the transition from one KO to the next. A change in the sign of the magnetic field at the transition from one CM to the next in a particular longitude interval on the longitude diagram indicates the formation of a new magnetic flux in this interval, and hence the destruction of the old and formation of a new structure. A change in the magnetic field strength without a change in the sign of its polarity does not affect the structural organization of the GMF and is not taken into account when calculating KLON. In total, there are 72 longitude intervals in each CM, according to WSO data (360 deg., full longitude interval, divided by 5 deg. intervals of WSO data). The KLON calculation analyzes magnetic fields in two consecutively adjacent CMs at each longitude at 5 degree intervals. The KLON coefficient is calculated as the ratio of the number of longitudes in which a polarity change occurred during the transition from one CM to the next to the total number of longitude intervals in the CM (72) [Bilenko, 2014]. Thus, the KLON coefficient shows in which number of longitude intervals the sign of magnetic field changed, i.e., a new magnetic flux is observed, and in which it remained unchanged. If the KLON coefficient remains at approximately the same low level for several RCs, it means that the KLON change rate is small and the structure of the GMF is practically unchanged, and if the KLON coefficient increases sharply, it means that a significant new magnetic flux has appeared and the rate of change in the magnetic field distribution is increasing, and the structural organization of the GMF is disturbed.

The longitude structurization of the GMF is clearly seen in Fig. 1c, which shows the longitude distribution of magnetic fields at the source surface, but this structure is poorly manifested at the photospheric level (Fig. 1a). To prove that the longitude distribution of magnetic fields is not random, we tested their distributions for randomness. A widely used test for the randomness of the series distribution is the autocorrelation criterion. One of the effective modifications of the

autocorrelation criterion is the criterion of the sum of the correlation coefficients of the first and second orders [Knoke, 1975]:

$$r_A = \frac{\sum_{i=1}^{n-1}(x_i - \bar{x})(x_{i+1} - \bar{x}) + \sum_{i=1}^{n-2}(x_i - \bar{x})(x_{i+2} - \bar{x})}{\sum_{i=1}^{n}(x_i - \bar{x})^2}$$

At confidence probability α=0.95, the interval of critical values for a random distribution of the series of 72 values is from -0.21 to 0.18. The values obtained for both large-scale photospheric magnetic fields and fields calculated at the source surface are significantly higher than the upper limit of the specified interval (thin horizontal line in Fig. 2e), which indicates their non-random distribution.

Since the distribution of magnetic fields in the CM does not obey a strictly normal distribution, we checked the series for the randomness of the distribution by the Wald-Wolfowitz rank test [Wald and Wolfowitz, 1943]:

$$r_W = \sum_{i=1}^{n-1}\left(R_i - \frac{n+1}{2}\right)\left(R_{i+1} - \frac{n+1}{2}\right)$$

Given

$$\frac{|r_W|}{\sqrt{D(r_W)}} > u_{\frac{1+\alpha}{2}}$$

where

$$D(r_W) = \frac{n^2(n+1)(n-3)(5n+6)}{720}$$

with probability α the hypothesis of randomness of the series is rejected. When α=0.95 u=1.96. The corresponding plots shown in Fig. 2f confirm the non-random character of the distribution of magnetic fields by longitude, since the calculated values of $r_W$ for both the CFMP and the fields calculated at the source surface are much higher than u=1.96 (thin horizontal line in Fig. 2f).

## 4. DEPENDENCES OF MAGNETIC FIELD STRENGTHS ON THE RATE OF THEIR STRUCTURAL CHANGES

Fig. 3 shows the dependences of the average magnetic field strength in each CM on the KLON coefficient, which characterizes the degree of chaotic structure of the magnetic field, for the entire period of consideration as a whole (Figs. 3a1-a3) and separately for each cycle. Both in general for the entire period under study and in each individual cycle, a decrease in the average magnetic field strength in the KO with increasing KLON is observed. In [Bilenko and Tavastsherna, 2017], it was shown for 21-23 cycles that the more stable the HMP structure, i.e., the lower the KLON, the higher the magnetic field strength in the cycle. From Fig. 2 and Fig. 3 also show that the KLON values are

higher in cycles 23, 24, and 25, i.e., in weak cycles with lower average over-KO magnetic field values, than in high, 21, and 22 cycles. The histograms of these dependences for the number of the corresponding CMs and the mean per CM values of the magnetic fields of positive and negative polarity are shown in Figs. 4 and 5, from which it follows that KLON does not exceed approximately 0.2 in the majority of CMs. Decrease of values on the histograms at KLON growth does not occur smoothly and gradually, but additional increases and decreases are observed. For the histogram of the KO number there is a growth in the KLON region of about 0.15-0.4 in all cycles. It should be noted that the histograms for the dependences of the mean per KO dependences of the positive and negative magnetic fields on KLON differ significantly, which is especially clear in the high 21st and 22nd cycles. In cycle 22, an increase in the KLON region of about 0.35 is observed (Fig. 5c1), which is more pronounced in the dependence for magnetic fields of negative polarity (Fig. 5c3).

## 5. COMPARISON OF CYCLIC CHANGES OF THE STRUCTURE OF THE GLOBAL MAGNETIC FIELD OF THE SUN WITH VARIATIONS OF HARMONICS OF THE SPHERICAL HARMONIC ANALYSIS

As was shown in [Chapman and Bartels, 1940; Altschuler and Newkirk, 1969; Altschuler et al., 1975], the solar magnetic field can be described as a function of the coordinates of radius, latitude, and longitude ($r$, $\theta$, $\varphi$):

$$f(r,\theta,\varphi) = Rs \sum_{n=1}^{N}\sum_{m=0}^{n}\left(\frac{Rs}{r}\right)^{n+1}[g_n^m \cos(m\varphi) + h_n^m \sin(m\varphi)]\, P_n^m(\theta),$$

where: $Rs$ is the radius of the Sun; $P_n^m(\theta)$ is the attached Lejandre polynomials; $N$ is the number of harmonics; the coefficients: $g_n^m, h_n^m$ - are calculated by fitting by the method of least squares the observed radial component of the photospheric magnetic field in the potential approximation. This method allows us to represent the magnetic field as a sum of separate harmonics. Each harmonic calculated according to certain indices (n, m) corresponds to the contribution of magnetic fields of different structural scales to the total distribution. From the values of the coefficients $g_n^m, h_n^m$ one can obtain the power spectrum of different harmonics [Altschuler et al., 1977; Levine, 1977]:

$$S_n = \sum_{m=0}^{n}[(g_n^m)^2 + (h_n^m)^2].$$

The distribution of magnetic fields at m = 0 corresponds to the zonal structure of the GMF distribution with a characteristic alternating distribution of intervals of magnetic fields of positive and negative polarity along the latitude. The zonal structure describes the axisymmetric components of the GMF. It can be symmetric or antisymmetric with respect to the Sun's equator. There can be n-m+1 zones in total. At n = m, the structure of the GMF is called sectoral. It is characterized by the formation of alternating meridional regions of magnetic fields of positive and negative polarity.

Under the condition n ≠ m ≠ 0, the harmonics are called tesseral. The distribution of magnetic fields in this case is an alternation on the sphere of quadrants of positive and negative polarity or spherical triangles, if we are talking about polar zones.

Fig. 6 shows the cyclic variations of the different harmonics of the spherical harmonic analysis of the HMP. Fig. 6a shows the variations of the sum of sector harmonics (n= m). The sum of the zonal harmonics at n = 1, 3, ..., 9 and m = 0 is shown in Fig. 6b (thin line, $\Sigma SZON1$), and at n= 2, 4, ..., 8 and m= 0 - in Fig. 6b (thick line, $\Sigma SZON2$). Since the intensity of zonal harmonics at even "n" is much lower than at odd "n", and they appear only at the maximum of each cycle, their contribution to the total value of zonal harmonics (Fig. 6c) is noticeable only during the periods of maximum spot activity, and at the rest of the time it is negligible. Therefore, the course of the total value of zonal harmonics is determined by harmonics with n= 1, 3, ..., 9 and m= 0. The evolution of individual harmonic components was considered in detail in Refs: [Hoeksema and Scherrer, 1986], [Bilenko and Tavastsherna, 2016, 2017], [Obridko, Shibalova and Sokoloff, 2023, 2024]. The change in the ratio of the sum of sectoral and zonal harmonics in cycles 21-25 is shown in Fig. 6d. The periods of dominance of sectoral structures are marked in gray. One should note a sharp increase in the role of sectoral structures in the weak, 23-25 cycles, compared to the high, 21 and 22 cycles. This corresponds to the growth of KLON (Fig. 2d) in cycles 23-25. Apparently, it is the growth of the fraction of sectoral structures and randomness (growth of the values of KLON) that leads to a decrease in the mean CM magnetic field strength in these cycles. The excess of the sum of zonal harmonics even in the periods of their dominance (highlighted in white) is insignificant. In [Obridko, Shibalova and Sokoloff, 2024], the role of tesseral harmonics was noted, (n ≠ m ≠ 0) whose contribution in solar activity maxima can be up to 60-65%. Fig. 6e shows variations of the tesseral harmonic with n= 6 and m= 3. By its structure, this harmonic can be one of the components in the dynamics of the sectoral structures of the HMP. For most tesseral harmonics, their amplitudes are significantly higher in the high, 21 and 22, than in the low, 23-25, cycles. Although for a number of tesseral harmonics, an increase is observed in cycle 25. Fig. 6f shows the polar (thick line) and equatorial (thin line) dipole variations. The intensity of the equatorial dipole is higher during the periods of dominance of the sectoral structure of the HMP in each cycle, and it decreases from high, 21-22, cycles to 24, and then there is a still small but increasing increase in cycle 25. The variations of the polar dipole in cycles correspond to the identified and described above alternation of the dominance of the polarity of the magnetic field in the structures in even and odd cycles. It is possible that the total contribution of cyclic variations of the magnetic fields of the polar dipole, the sum of sectoral harmonics and tesseral harmonics with even values of n and odd values of m are determinants in the formation and cyclic variations of the observed sectoral structure of the HMP.

## 6. CONCLUSIONS

Changes in the structure of the HMP in cycles 21-24 and the beginning of cycle 25 from May 1976 to December 2024 inclusive (1642-2292 KO) have been considered.

It is shown that the size, duration of quasi-stable existence, character of rotation, and tension in each individual unipolar structure are different in different cycles and in the phases of minimum, growth, maximum, and decline of each individual cycle. These structures are characterized by rotation with the period of KO, which may indicate their connection with local magnetic fields.

In each separate structure, two extended longitude intervals are distinguished, one of which is dominated by magnetic fields of positive polarity and the other by negative polarity, occupying approximately opposite longitude intervals, which alternate in even and odd cycles.

The KLON values, which characterize the degree of chaotic structure of the magnetic field, are higher in 23, 24, and 25, i.e., in weak cycles, than in high, 21 and 22 cycles. This corresponds to the periods of growth of the contribution of sectoral structures, which in total leads to a decrease in the mean values of magnetic field strengths in these cycles.

The histograms for the dependences of positive and negative magnetic fields on KLON differ significantly, which is especially clear in the high, 21, and 22 cycles, indicating a difference in their structural organization and dynamics.

It is proposed as an explanation that the total contribution of the cyclic variations of the magnetic fields of the polar dipole, the sum of sectoral harmonics and tesseral harmonics with even values of $n$ and odd values of $m$ are the determinants in the formation and cyclic variations of the observed sectoral structure of the HMP.

## ACKNOWLEDGEMENTS

The study was conducted under the state assignment of Lomonosov Moscow State University.

Wilcox Solar Observatory data used in this study was obtained via the web site http://wso.stanford.edu at 2025:01:28_12:04:38 PST courtesy of J.T. Hoeksema. Hoeksema. The Wilcox Solar Observatory is currently supported by NASA.

## FUNDING

This work was funded by the budget of the P.K. Sternberg State Astronomical Institute of Lomonosov Moscow State University. No additional grants were received to conduct or supervise this particular study.

## CONFLICT OF INTERESTS

The author of this paper declares that she has no conflict of interest.

REFERENCES


1. *Altschuler M.D. and Newkirk G.Jr*. Magnetic fields and the structure of the solar corona // Solar Phys. V. 9. P. 131–149. 1969.
2. *Altschuler M.D., Trotter D.E., Newkirk G.Jr. and Howard R*. Tabulation of the harmonic coefficients of the solar magnetic fields // Solar Phys. V. 41. P. 225–226. 1975.
3. *Altschuler M.D., Levine R.H., Stix M. and Harvey J.* High resolution mapping of the magnetic field of the solar corona // Solar Phys. V. 51. P. 345–375. 1977.
4. *Ambrož P., Bumba V., Howard R. and Sýkora J*. Opposite polarities in the development of some regularities in the distribution of large-scale magnetic fields // IAUS. V. 43. P. 696–709. 1971.
5. *Bilenko I.A.* Influence of the solar global magnetic-field structure evolution on CMEs // Solar Phys. V. 289. P. 4209–4237. 2014.
6. *Bilenko I.A. and Tavastsherna K.S.* Coronal hole and solar global magnetic field evolution in 1976 – 2012 // Solar Phys. V. 291. P. 2329–2352. 2016.
7. *Bilenko I.A. and Tavastsherna K.S*. Coronal holes as tracers of the Sun's global magnetic field in cycles 21–23 of solar activity // Geomagn. Aeronomy. V. 57. N. 7. P. 803–813. 2017.
8. *Bilenko I.A.* Manifestation of Rossby waves in the global magnetic field of the Sun during cycles 21–24 // Astrophys. J. Letters. V. 897. L24 (5 pp). 2020.
9. *Bumba V. and Howard R*. Solar activity and recurrences in magnetic field distribution // Solar Phys. V. 7. P. 28–38. 1969.
10. *Bumba V. and Obridko V. N.* 'Bartels' active longitudes', sector boundaries and flare activity // Solar. Phys. V. 6. P. 104–110. 1969.
11. *Bumba V*. Large-scale solar magnetic fields // IAUS. V. 71. P. 47–67. 1976.
12. *Chapman S. and Bartels J.* Geomagnetism. V. 2. Oxford. 1050 p. 1940.
13. *Hoeksema J.T. and Scherrer P.H.* An atlas of photospheric magnetic field observations and computed coronal magnetic fields: 1976–1985 // Solar Phys. V. 105. P. 205–211. 1986.
14. *Hoeksema J.T.* large-scale solar and heliospheric magnetic fields // Adv. Space Res. V. 11. P. 15–24. 1991.
15. *Insley J.W., Moore V. and Harrison R.A.* The differential rotation of the corona as indicated by coronal holes // Solar Phys. V. 160. P. 1–18. 1995.
16. *Ivanov E.V. and Obridko V.N.* Role of the large–scale solar magnetic field structure in the global organization of solar activity // Geomagn. Aeronomy. V. 54. N. 8. P. 996–999. 2014.
17. *Fainshtein V.G. and Ivanov E.V.* Relationship between CME parameters and large-scale structure of solar magnetic fields // Sun Geosphere. V. 5. 28–33. 2010.

18. *Knoke J.D.* Testing for randomness against autocorrelation: The parametric case // Biometrika. V. 62. P. 571–575. 1975.
19. *Levine R.H.* Evolution of photospheric magnetic field patterns during SKYLAB // Solar Phys. V. 54. P. 327–341. 1977.
20. *McIntosh P.S.* Patterns and dynamics of solar magnetic fields and He I coronal holes in cycle 23 // International Solar Cycle Studies Symposium SP–535, ESA. P. 807–818. 2003.
21. *Obridko V.N. and Shelting B.D.* Coronal holes as indicators of large-scale magnetic fields in the corona // Solar Phys. V. 124. P. 73–80. 1989.
22. *Obridko V.N., Shibalova A.S. and Sokoloff D.D*. The extended solar cycle and asymmetry of the large-scale magnetic field // MNRAS. V. 523. P. 982–990. 2023.
23. *Obridko V.N., Shibalova A.S. and Sokoloff D.D.* Cyclic variations of the structure and energetics of solar magnetic fields // MNRAS. V. 529. P. 2846–2853. 2024.
24. *Sanchez-Ibarra A. and Barraza-Paredes M.* Catalog of coronal holes, 1970–1991, Report UAG–102, Boulde: World Data Center A for solar-terrestrial physics, National Geophysical Data Center, 1992.
25. *Tikhomolov E*. Rossby vortices as sources of global magnetic structures on the Sun // Solar Phys. V. 156. P. 205–219. 1995.
26. *Wald A. and Wolfowitz J.* An exact test for randomness in the non parametric case based on
27. serial correlation // AMS. V. 14. P. 378–388. 1943.
28. *Zhao, Xuepu and Hoeksema J.T.* Unique determination of model coronal magnetic fields using photospheric observations // Solar. Phys. V. 143. P. 41–48. 1993.
29. *Zherebtsov G.A., Kovalenko V.A. and Molodykh S.I.* Heliospheric characteristics during fast global variations of solar magnetic fields // J. Geophys. Res. V. 102. P. 2137-2146. 1997.

**Table 1.**

| N | t (KO) | L+ (deg.) | L- (deg.) | Bmax+ (μT) | Bmin- (μT) |
|---|---|---|---|---|---|
| 21 cycle. | | | | | |
| 1 | 1694-1719 | 0-105, 245-360 | 105-245 | 11.76 | -9.71 |
| 2 | 1720-1745 | 0-150 | 150-360 | 10.24 | -18.24 |
| 3 | 1746-1770 | 100-315 | 0-230, 310-360 | 5.75 | -7.41 |
| 22 cycle | | | | | |
| 4 | 1800-1838 | 90-270 | 0-90, 270-360 | 14.53 | -12.91 |
| 5 | 1839-1856 | 200-360 | 0-200 | 12.20 | -16.14 |
| 6 | 1857-1873 | 0-115, 270-360 | 115-270 | 5.97 | -4.66 |
| 23 cycle | | | | | |
| 7 | 1952-1970 | 0-150, 315-360 | 150-315 | 8.05 | -8.11 |
| 8 | 1971- 1983 | 80-250 | 0-80, 250-360 | 7.94 | -6.59 |
| 9 | 1984-2023 | 0-200 | 200-360 | 10.29 | -9.99 |
| 24 cycle | | | | | |
| 10 | 2096-2119 | 0-90, 200-360 | 90-200 | 4.84 | -4.83 |
| 11 | 2120-2144 | 0-250, 300-360 | 0-130, 220-315 | 5.38 | -6.38 |
| 12 | 2145-2190 | 0-45, 200-360 | 45-200 | 10.58 | -7.61 |
| 25 cycle | | | | | |
| 13 | 2240-2264 | 100-270 | 0-100, 270-360 | 7.32 | -6.1 |
| 14 | 2265-2292 | 0-200, 300-360 | 200-300 | 6.81 | -6.56 |

## FIGURE CAPTIONS

**Fig. 1.** Longitude-temporal distribution diagrams of (a) CPMF, (b) CPMF averaged over 9 CMs, (c) magnetic field calculated at the source surface (2.5 Rs). The longitude structures, whose parameters are given in Table 1, are marked with figures.

**Fig. 2.** Cyclic variations of (a) KFMP strength, (b) KFMP strength averaged over 9 KOs, (c) magnetic field strength calculated at the source surface (2.5 Rs). (d) KLON cyclic variations. Thin lines indicate the averages for each KO, and thick solid lines (and dashed lines for the magnetic field moduli) indicate the values averaged over the 13 KOs. (e) Results of the test for the randomness of the longitude distribution of magnetic fields calculated by the autocorrelation method for the longitude diagram data of Fig. 1a (arrow Phot.) and Fig. 1c (arrow 2.5 Rs). The

thin horizontal line marks the upper limit of the critical value interval under random distribution at α=0.95. (f) Results of the test for the randomness of the longitude distribution of magnetic fields obtained using the Wald-Wolfowitz rank method for the longitude diagram data of Fig. 1a (arrow Phot.) and Fig. 1c (arrow 2.5 Rs). The thin horizontal line marks the critical level u=1.96 at α=0.95. The periods of dominance of the sectoral structure of the HMP in each cycle are marked in gray. The maximum and minimum moments of each cycle are shown at the top.

**Fig. 3.** Dependences of positive (a2-f2), modulus of negative (a3-f3) and sum of moduli of positive and negative (a1-f1) magnetic fields at the source surface on KLON. (a1-a3) - dependencies for the data for the whole period under consideration. (b1-f3) - dependences separately for 21-25 cycles.

**Fig. 4.** Histograms of dependences of the number of KOs on KLON for the sum of the moduli of the magnetic fields of positive and negative polarity shown in Figs. 3a1-f1.

**Fig. 5.** Histograms of the dependencies of magnetic fields on KLON shown in Fig. 3.

**Fig. 6.** Variations of (a) sum of sectoral harmonics (n= m); (b) sum of zonal harmonics (n= 1, 3, ..., 9, m= 0, thin line, $\Sigma S_{ZON1}$) and sum of zonal harmonics (n= 2, 4,...8, m= 0, thick line, $\Sigma S_{ZON2}$); (c) sum of zonal harmonics (n= 1, 2, 3, .. ..., 9, m= 0); (d) ratio of the sum of sectoral to the sum of zonal harmonics; (e) tesseral harmonic with n= 6 m= 3; (f) polar dipole (thick line) and equatorial dipole (thin line) variations. The periods of dominance of the sectoral structure of the HMP in each cycle are marked in gray. The maximum and minimum moments of each cycle are shown at the top.

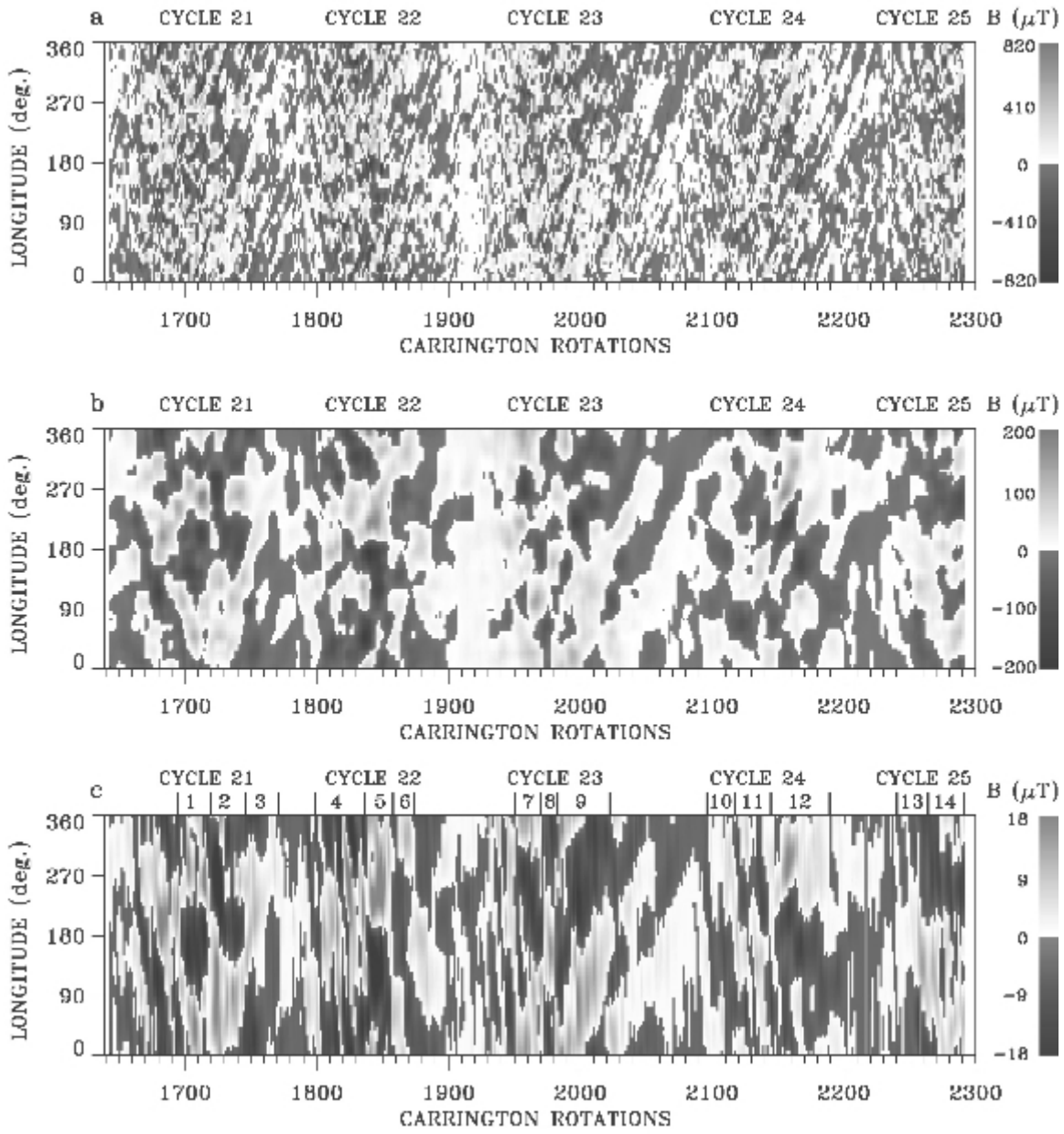
a
CYCLE 21
CYCLE 22
CYCLE 23
CYCLE 24
CYCLE 25
B (μT)
820
410
0
-410
-820
LONGITUDE (deg.)
360
270
180
90
0
1700
1800
1900
2000
2100
2200
2300
CARRINGTON ROTATIONS
b
CYCLE 21
CYCLE 22
CYCLE 23
CYCLE 24
CYCLE 25
B (μT)
200
100
0
-100
-200
LONGITUDE (deg.)
360
270
180
90
0
1700
1800
1900
2000
2100
2200
2300
CARRINGTON ROTATIONS
c
CYCLE 21
CYCLE 22
CYCLE 23
CYCLE 24
CYCLE 25
1
2
3
4
5
6
7
8
9
10
11
12
13
14
B (μT)
18
9
0
-9
-18
LONGITUDE (deg.)
360
270
180
90
0
1700
1800
1900
2000
2100
2200
2300
CARRINGTON ROTATIONS

Fig. 1.

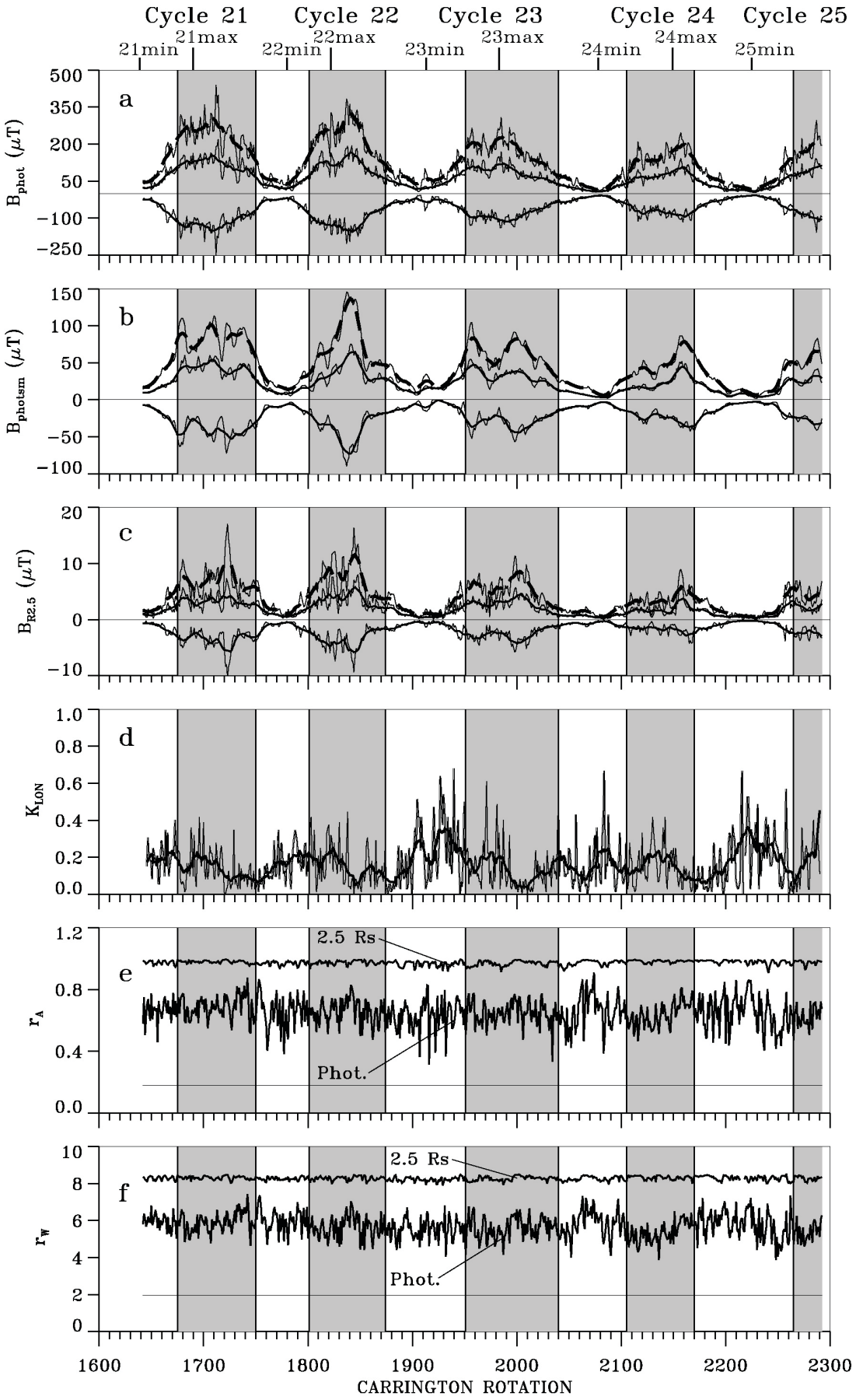
Cycle 21
Cycle 22
Cycle 23
Cycle 24
Cycle 25
21min
21max
22min
22max
23min
23max
24min
24max
25min
a
b
c
d
e
f
$B_{phot}$ ($\mu$T)
$B_{photsm}$ ($\mu$T)
$B_{R2.5}$ ($\mu$T)
$K_{LON}$
$r_A$
$r_W$
2.5 Rs
Phot.
CARRINGTON ROTATION

Fig. 2.

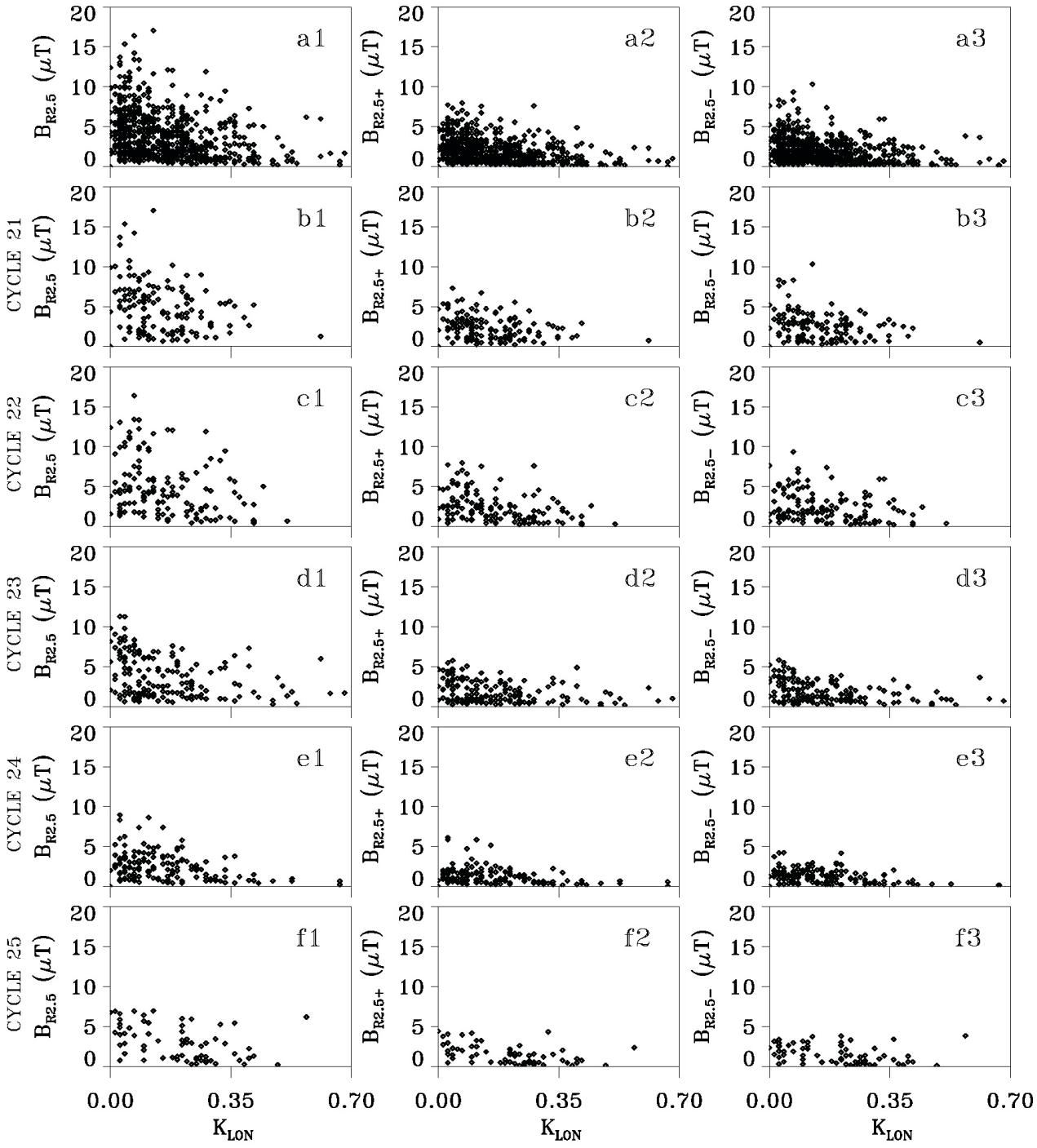
a1
a2
a3
b1
b2
b3
c1
c2
c3
d1
d2
d3
e1
e2
e3
f1
f2
f3
CYCLE 21
CYCLE 22
CYCLE 23
CYCLE 24
CYCLE 25
B_R2.5 (μT)
B_R2.5+ (μT)
B_R2.5- (μT)
0
5
10
15
20
0.00
0.35
0.70
K_LON

Fig. 3.

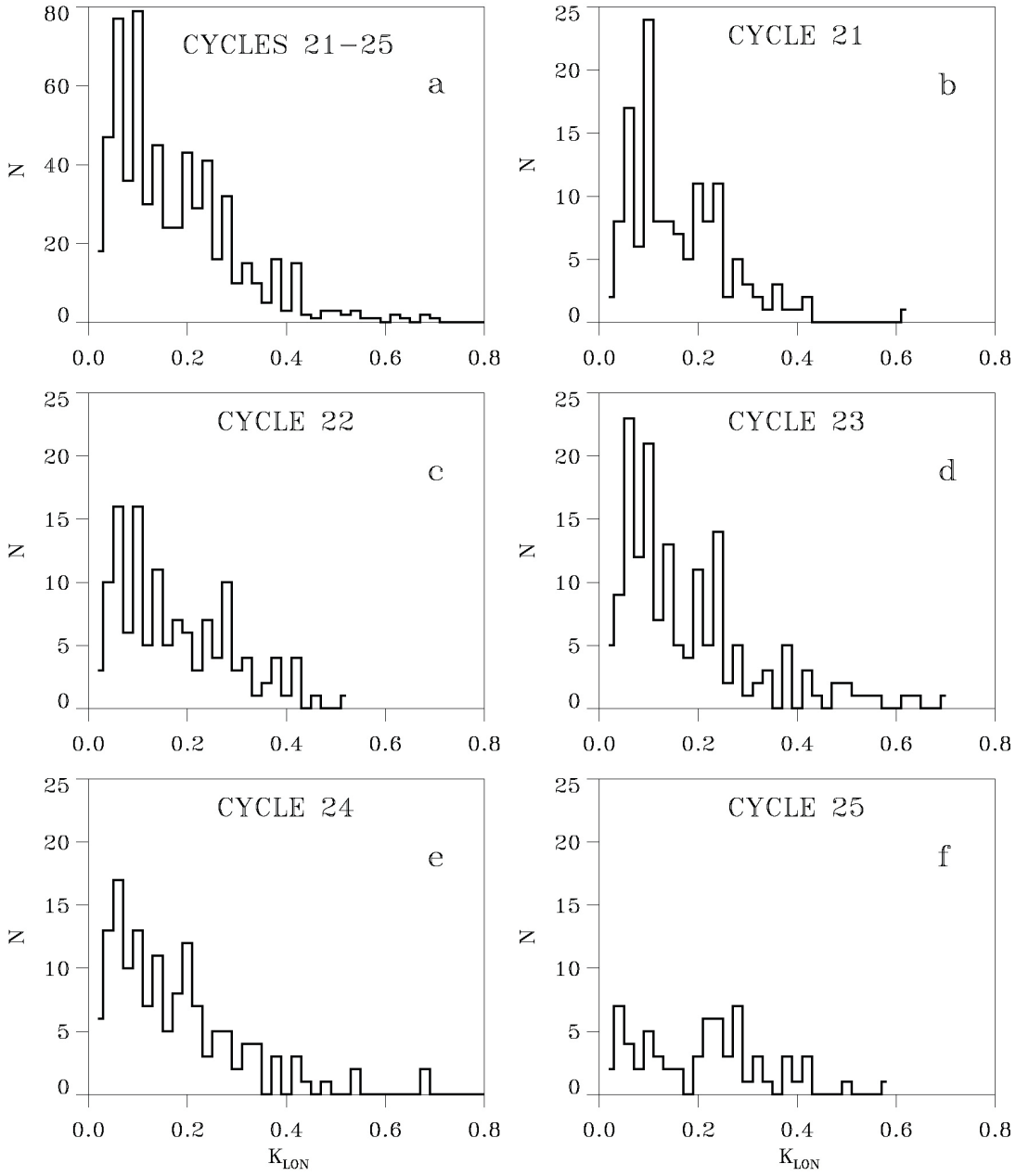
CYCLES 21–25
a
CYCLE 21
b
CYCLE 22
c
CYCLE 23
d
CYCLE 24
e
CYCLE 25
f
N
$K_{LON}$

Fig. 4.

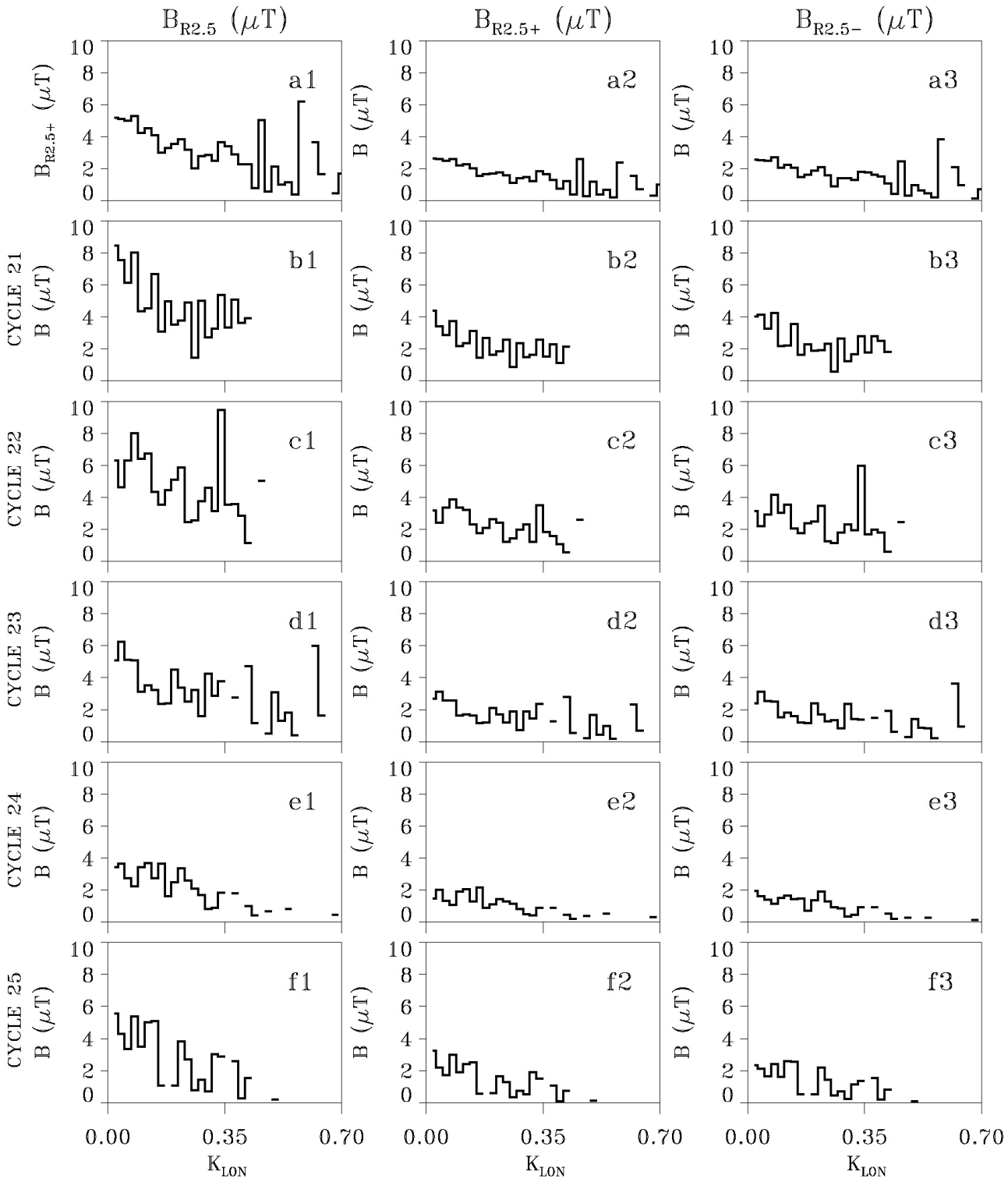
B_R2.5 (μT)
B_R2.5+ (μT)
B_R2.5− (μT)
a1
a2
a3
b1
b2
b3
c1
c2
c3
d1
d2
d3
e1
e2
e3
f1
f2
f3
CYCLE 21
CYCLE 22
CYCLE 23
CYCLE 24
CYCLE 25
B (μT)
0 2 4 6 8 10
0.00 0.35 0.70
K_LON

Fig. 5.

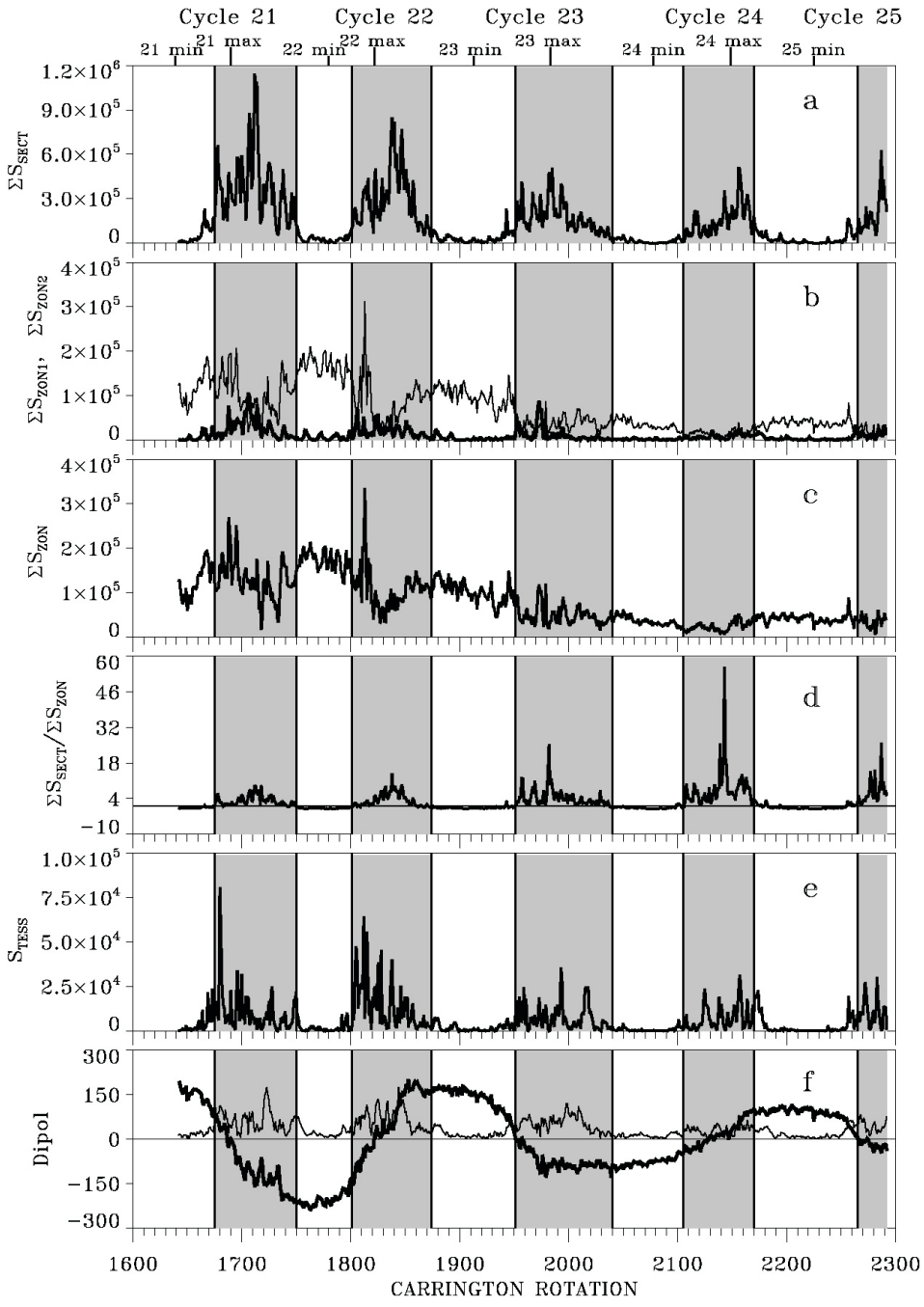
Cycle 21
Cycle 22
Cycle 23
Cycle 24
Cycle 25
21 min
21 max
22 min
22 max
23 min
23 max
24 min
24 max
25 min
a
b
c
d
e
f
$\Sigma S_{SECT}$
$\Sigma S_{ZON1}$, $\Sigma S_{ZON2}$
$\Sigma S_{ZON}$
$\Sigma S_{SECT}/\Sigma S_{ZON}$
$S_{TESS}$
Dipol
CARRINGTON ROTATION

Fig. 6.